On the foundation dynamics and the active control of flexible rotors via active magnetic bearings

T. T. Paulsen, I. F. Santos
Department of Mechanical Engineering Technical University of Denmark, Denmark

ABSTRACT

A high-speed blower consisting of a flexible shaft supported by two radial active magnetic bearings and an axial passive magnetic bearing is theoretically and experimentally analysed. The blower is mounted on a t-slot plate and the interactions between the shaft, the housing, and the t-slot plate are under consideration. It is investigated if the dynamical contribution from the foundation dynamics (t-slot plate plus housing) to the frequency response function of the high-speed blower can be reduced by including some of the most influential dynamics (mode shapes) of the foundation in the control object using a model-based control design.

MATHEMATICAL PARAMETERS

α – Proportional damping for mass
β – Proportional damping for stiffness
μ_0 – Permeability for vacuum
$\omega_{0,1}$ – Cross frequency for notch filter 1
$\omega_{0,2}$ – Cross frequency for notch filter 2
A – Surface area for pole legs
i_0 – Operating current in coils
N – Number of turns for coils
Q – Stop band factor for notch filter
R – Ohmic resistance
x_0 – Operating air gap in bearings
$\mathbf{x}$ – Vector x (bold small letter)
$\mathbf{X}$ – Matrix x (bold capital letter)
$[\ ]_{Axial}$ – Axial magnetic bearing related
$[\ ]_b$ – Boundary nodes
$[\ ]_{CB}$ – Craig-Bampton related
$[\ ]_{ext}$ – External related
$[\ ]_f$ – Foundation related
$[\ ]_i$ – Internal nodes
$[\ ]_{int}$ – Integral states augmented
$[\ ]_l$ – Left side transformation
$[\ ]_{MR}$ – Modal reduction related
$[\ ]_{n\times m}$ – n row and m column matrix
$[\ ]_{obj}$ – Control object
$[\ ]_r$ – Rotor related
$[\ ]_{ref}$ – Reformulated matrix
$[\ ]_{ri}$ – Right side transformation
$[\ ]_{ss}$ – State space related

1 INTRODUCTION

The number of industrial applications exploiting magnetic bearing technology is increasing. Some of the great advantages in favour of the technology are low friction, low maintenance, low to zero wear during start-up and run-down, and customisable frequency response. Some setbacks for the technology are the complexity and cost (1). For specific applications, the advantages are overwhelming. These applications have helped develop the magnetic bearing technology into how it is used today. The load carrying capabilities of magnetic bearings have been increasing due to this development. This has led to an increasing number of applications adopting

magnetic bearing technology. In (2), the capabilities of the active magnetic bearing technology taking form at that time is discussed. An example of researchers trying to push the limits on carrying capacities of the technology using novel configurations is presented in (3).

For rotating machinery, some sort of support used to fixate the structure to the ground is necessary. If the support structure is flexible within the speed range of the machine it is fixating, process disturbances or residual unbalance could excite the flexible support structure. Interactions between beams or rotors and support structures or foundations are a familiar problem as presented in (4-7) among others. As the carrying capabilities for the magnetic bearing technology is increasing, so is the weight of the machines it is used for. Therefore, a greater support structure is needed. In general, the change of the mass will be more dominant than the change in stiffness for a structure as it is scaled, if the structure is not wisely designed. Therefore, if the foundation of a machine is increased in size, the flexible modes for that foundation will be lowered. Combined with the higher reaction forces needed for the magnetic bearings to support the rotor used in the machine, the flexible modes for the foundation are more likely to be excited through disturbances in the rotor within the operational speed range of the machine.

For other applications, a reduction to the total weight of the machine is desired, though the inertia of a spinning element will still be considerable. In this case, the support structure will be flexible if it is not carefully designed. Furthermore, for some applications a soft interaction between the machine housing and the machine carrier is considered an opportunity (8). This can result in amplifications of the dynamical response due to external disturbances.

If a machine were to comply with ISO 10349-1, a threshold for the mechanical vibration amplifications within the speed range of the machine is specified. If the specified threshold cannot be satisfied, the speed range will have to be compromised, else a reduction in the amplifications should be considered.

In this article, the dynamical impact from the foundation of a high-speed blower without an impeller mounted, thereby neglecting the fluid forces, is considered. The high-speed blower is investigated both mathematically and experimentally.

The experimental test setup, described in (9), consists of a rotor, an axial passive magnetic bearing, two radial active magnetic bearings, and an induction motor. The bearings and the motor are situated in a housing that is mounted to a t-slot plate. The housing and the t-slot plate is referred to as the foundation. To establish the mathematical model used to simulate the high-speed rotor interacting with the foundation, two finite element method models have been formulated, i.e. one for the rotor and one for the foundation. The interactions between the rotor and the foundation are described through a linearized mathematical model of the bearing dynamics.

In this work, a Proportional and Integral (PI) control law is used for the amplifiers to track a current reference defined by a position control law. Initially, the position control law is a Proportional, Integral, and Derivative (PID) control law using two notch filters applied to the position sensor signal. From this setup, an identification procedure for the estimated interaction coefficients can be carried out.

Using the identified bearing coefficients, model-based control laws can be used to generate the current reference signal. This will allow the control law to utilize the mathematical model conducted to help the controller place meaningful gains in the frequency domain to counteract undesired resonating peaks from the rotor-bearing-foundation interaction. Here, a Linear Quadratic Gaussian (LQG) control law using full state feedback with a Kalman filter as observer has been chosen. The PID control law will be compared against the LQG control law approach to investigate if this method is good at reducing the undesired amplifications in the frequency range.

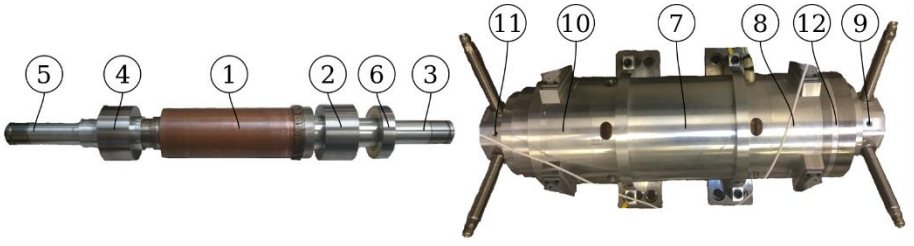

Figure 1: Presentation of high-speed blower test facility components with included features. The shaft has a copper sheet, ①, a pair of rotor laminate stacks, ② and ④, aluminium surfaces for sensors, ③ and ⑤, and a disc with passive magnets, ⑥. The housing consists of an induction motor, ⑦, a pair of radial AMB stator geometries, ⑧ and ⑩, eddy current sensor fitting modules, ⑨ and ⑪, and axial PMB, ⑫.

Table 1: Values for AMB design.

Parameter	N	R	A	i_0	x_0
Value	78 [−]	0.8 [Ω]	754 [mm^2]	4 [A]	0.45 [mm]

2 EXPERIMENTAL TEST FACILITY

The experimental test facility representing a high-speed blower, presented in figure 1**,** consists of a rotor and a housing. The rotor and housing are equipped with hardware components used to facilitate the use of Active Magnetic Bearings (AMBs) for a high-speed blower. An induction motor is used to rotate the shaft; two AMB geometries are used to control the shaft position with the help of four eddy current sensors. An axial Passive Magnetic Bearing (PMB) is used to keep the shaft approximately centred in the axial direction during test runs. The design parameters for the AMBs implemented in the high-speed blower are provided in table 1.

2.1 Experimental investigations

The conducted experiments and theoretical analysis are based on an initial study for the high-speed blower controlled using a PID controller implemented with two notch filters on the position sensor signals for stabilizing the first flexible mode of the shaft. The linearized coefficients for the AMBs have been optimized through a system identification procedure similar to the one described in (10). The frequency response obtained experimentally is compared to that expected from the control object. The experimentally obtained frequency response using the PID control design is then compared to the frequency response generated from the LQG control design considering the most influential foundation dynamical response in the control objective. The comparison is carried out with the rotor of the high-speed blower levitated without the rotor spinning. A Campbell diagram and unbalance response are simulated for both cases and the results are compared.

3 MATHEMATICAL MODEL

The global mathematical model is described from a combination of mathematical models for the components included in the high-speed blower test facility. The mathematical models include a Finite Element Model (FEM) of the shaft, a FEM of the foundation, linearized expressions for the dynamics within the AMBs and the PMB, filters applied to sensor signals, and control schemes implemented to the control objective. In figure 2, an overview of the connections established between the different mathematical models is available. Also, the implemented model-based

control design is presented in the figure. The construction of the mathematical model is also presented in (9). The rotor model is formulated using Timoshenko beam elements described in (11) with the mathematical formulation of the dynamic response described by equation (1). The equation for the dynamical response is formulated into a system of first order differential equations in equation (3) with the matrices presented in equation (2).

$$\mathbf{M}_r\ddot{\mathbf{x}}_r + (\mathbf{D}_r - \omega\mathbf{G}_r)\dot{\mathbf{x}}_r + \mathbf{K}_r\mathbf{x}_r = \mathbf{f}_{r,ext} \quad (1)$$

$$\mathbf{A}_{r,ss} = \begin{bmatrix} \mathbf{0} & \mathbf{I} \\ -\mathbf{M}_r^{-1}\mathbf{K}_r & -\mathbf{M}_r^{-1}(\mathbf{D}_r - \omega\mathbf{G}_r) \end{bmatrix}, \mathbf{B}_{r,ss} = \begin{bmatrix} \mathbf{0} \\ \mathbf{M}_r^{-1} \end{bmatrix}, \mathbf{C}_{r,ss} = \begin{bmatrix} \mathbf{I} & \mathbf{0} \\ \mathbf{0} & \mathbf{I} \end{bmatrix}, \mathbf{D}_{r,ss} = \begin{bmatrix} \mathbf{0} \\ \mathbf{0} \end{bmatrix} \quad (2)$$

$$\mathbf{G}_{r,ss} = \begin{cases} \dot{\mathbf{x}}_{r,ss} = \mathbf{A}_{r,ss}\mathbf{x}_{r,ss} + \mathbf{B}_{r,ss}\mathbf{u}_{r,ss} \\ \mathbf{y}_{r,ss} = \mathbf{C}_{r,ss}\mathbf{x}_{r,ss} + \mathbf{D}_{r,ss}\mathbf{u}_{r,ss} \end{cases}, \quad \mathbf{x}_{r,ss} = \begin{Bmatrix} \mathbf{x}_r \\ \dot{\mathbf{x}}_e \end{Bmatrix}, \quad \mathbf{u}_{r,ss} = \{\mathbf{f}_{r,ext}\} \quad (3)$$

It is assumed that the damping present in the rotor can be described from proportional damping as formulated in equation (4).

$$\mathbf{D}_r = \alpha_r\mathbf{M}_r + \beta_r\mathbf{K}_r \quad (4)$$

The foundation is described using ANSYS Solid186 elements. The mathematical formulation for the foundation extracted from ANSYS consists of mass, $\mathbf{M}_f$, and stiffness, $\mathbf{K}_f$, matrices. These matrices are reduced using a Craig-Bampton reduction scheme. In equation (5), a reformulation, $\mathbf{M}_{f,red}$ and $\mathbf{K}_{f,\boldsymbol{red}}$, of the extracted matrices is presented. The reformulation describes the mass and stiffness matrices by a set of internal nodes, i, and a set of boundary nodes, b.

$$\mathbf{M}_{f,ref}\begin{Bmatrix} \ddot{\mathbf{u}}_i \\ \ddot{\mathbf{u}}_b \end{Bmatrix} + \mathbf{K}_{f,ref}\begin{Bmatrix} \mathbf{u_i} \\ \mathbf{u}_b \end{Bmatrix} = \mathbf{f}_{f,ref}, \quad \begin{bmatrix} \mathbf{M}_{f,i\times i} & \mathbf{M}_{f,i\times b} \\ \mathbf{M}_{f,b\times i} & \mathbf{M}_{f,b\times b} \end{bmatrix}\begin{Bmatrix} \ddot{\mathbf{u}}_i \\ \ddot{\mathbf{u}}_b \end{Bmatrix} + \begin{bmatrix} \mathbf{K}_{f,i\times i} & \mathbf{K}_{f,i\times i} \\ \mathbf{K}_{f,i\times i} & \mathbf{K}_{f,i\times i} \end{bmatrix}\begin{Bmatrix} \mathbf{u_i} \\ \mathbf{u}_b \end{Bmatrix} = \begin{Bmatrix} \mathbf{f}_{f,ext,i} \\ \mathbf{f}_{f,ext,b} \end{Bmatrix} \quad (5)$$

The reformulation is used to establish the reduction matrix, $\mathbf{R}$, presented in equation (6). The reduced eigenvector matrix, $\mathbf{V}_{i\times x}$, is calculated from solving the eigenvalue problem presented in equation (7) and choosing a number, x, of modes needing to be included in the reduced model.

$$\mathbf{R} = \begin{bmatrix} \boldsymbol{\Psi}_{i\times b} & \boldsymbol{\Phi}_{i\times x} \\ \mathbf{I}_{b\times b} & \mathbf{0}_{b\times x} \end{bmatrix}, \quad \boldsymbol{\Psi}_{i\times b} = -\mathbf{K}_{f,i\times i}^{-1}\mathbf{K}_{f,i\times b}, \quad \boldsymbol{\Phi}_{i\times x} = \mathbf{V}_{i\times x} \quad (6)$$

$$\boldsymbol{\Lambda}_{i\times i} = \mathbf{V}_{i\times i}^{-1}\mathbf{M}_{f,i\times i}^{-1}\mathbf{K}_{f,i\times i}\mathbf{V}_{i\times i} \quad (7)$$

For the Craig-Bampton reduction of the foundation, the number of modes is chosen as $x_{f,CB} = [1{:}\,100]$. The method for calculating the reduced mass, stiffness and damping matrices is presented in equation (8), assuming proportional damping. The system dynamics is then assumed to be described from equation (9). This dynamical relation can be formulated in state space as a first order system of differential equations in equation (11) with the matrices presented in equation (10).

$$\mathbf{M}_{f,red} = \mathbf{R}^{\mathrm{T}}\mathbf{M}_{f,ref}\mathbf{R}, \quad \mathbf{K}_{f,red} = \mathbf{R}^{T}\mathbf{K}_{f,ref}\mathbf{R}, \quad \mathbf{D}_{f,\boldsymbol{red}} = \alpha_f\mathbf{M}_{f,red} + \beta_f\mathbf{K}_{f,red} \quad (8)$$

$$\mathbf{M}_{\boldsymbol{f,red}}\ddot{\mathbf{x}}_f + \mathbf{D}_{\boldsymbol{f,red}}\dot{\mathbf{x}}_f + \mathbf{K}_{f,red}\mathbf{x}_f = \mathbf{f}_{f,ext} \quad (9)$$

$$\mathbf{A}_{f,ss} = \begin{bmatrix} \mathbf{0} & \mathbf{I} \\ -\mathbf{M}_{f,red}^{-1}\mathbf{K}_{f,red} & -\mathbf{M}_{f,red}^{-1}\mathbf{D}_{f,red} \end{bmatrix}, \mathbf{B}_{f,ss} = \begin{bmatrix} \mathbf{0} \\ \mathbf{M}_{f,red}^{-1} \end{bmatrix}, \mathbf{C}_{f,ss} = \begin{bmatrix} \mathbf{I} & \mathbf{0} \\ \mathbf{0} & \mathbf{I} \end{bmatrix}, \mathbf{D}_{f,ss} = \begin{bmatrix} \mathbf{0} \\ \mathbf{0} \end{bmatrix} \quad (10)$$

$$\mathbf{G}_{f,ss} = \begin{cases} \dot{\mathbf{x}}_{f,ss} = \mathbf{A}_{\boldsymbol{f},ss}\mathbf{x}_{f,ss} + \mathbf{B}_{f,ss}\mathbf{u}_{f,ss} \\ \mathbf{y}_{f,ss} = \mathbf{C}_{\boldsymbol{f},ss}\mathbf{x}_{f,ss} + \mathbf{D}_{f,ss}\mathbf{u}_{f,ss} \end{cases}, \quad \mathbf{x}_{f,ss} = \begin{Bmatrix} \mathbf{x}_f \\ \dot{\mathbf{x}}_f \end{Bmatrix}, \quad \mathbf{u}_{r,ss} = \{\mathbf{f}_{f,ext}\} \quad (11)$$

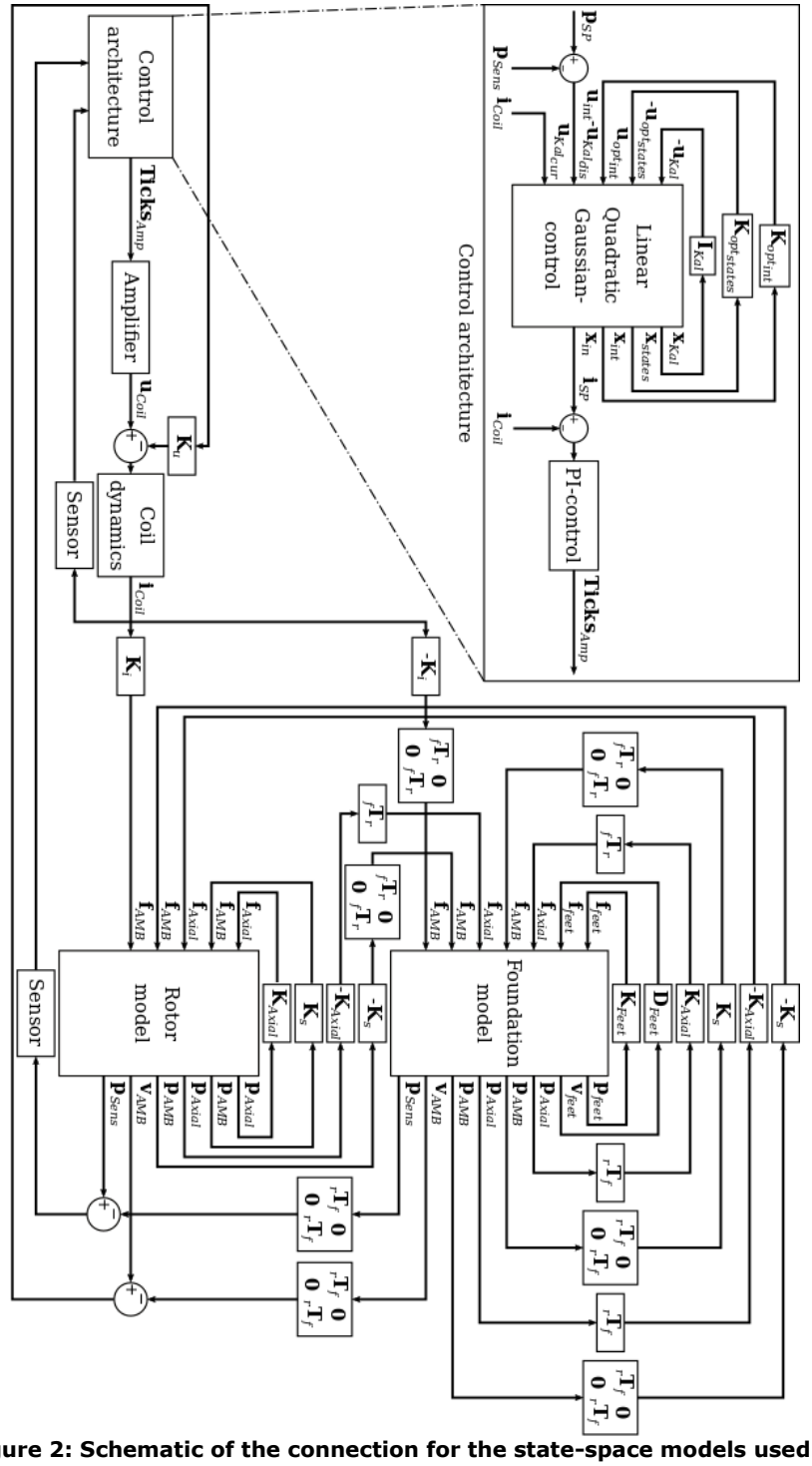

Figure 2: Schematic of the connection for the state-space models used to describe the system dynamics with implemented model-based controller.

The FEMs for the rotor and foundation are then both reduced using a modal reduction method. Two transformation matrices are deduced based on the eigenvalue problem for the model needing to be reduced, as presented in equation (12). A number, x, from a total number, n, of modes is chosen to establish the transformation. The reduced state space system is presented in equation (14) using the transformed matrices presented in equation (13).

$$\mathbf{\Lambda} = \mathbf{V}^{-1}\mathbf{A}_{ss}\mathbf{V}, \qquad \mathbf{T}_l = (\mathbf{V}^{-1})_{x\times n}, \qquad \mathbf{T}_{ri} = \mathbf{V}_{n\times x} \quad (12)$$

$$\bar{\mathbf{A}}_{ss} = \mathbf{T}_l\mathbf{A}_{ss}\mathbf{T}_{ri}, \qquad \bar{\mathbf{B}}_{ss} = \mathbf{T}_l\mathbf{B}_{ss}, \qquad \bar{\mathbf{C}}_{ss} = \mathbf{C}_{ss}\mathbf{T}_{ri} \quad (13)$$

$$\bar{\mathbf{G}}_{ss} = \begin{cases} \dot{\bar{\mathbf{x}}}_{ss} = \bar{\mathbf{A}}_{ss}\bar{\mathbf{x}}_{ss} + \bar{\mathbf{B}}_{ss}\mathbf{u}_{ss} \\ \mathbf{y}_{ss} = \bar{\mathbf{C}}_{ss}\bar{\mathbf{x}}_{ss} + \mathbf{D}_{ss}\mathbf{u}_{ss} \end{cases} \quad (14)$$

In this specific investigation, the number of modes for the shaft is chosen as $x_r = [1\ 2\ 3\ 4\ 5\ 6\ 7\ 8]$, which is describing the rigid body movements and the first two flexible modes in perpendicular directions. For the foundation, the modes $x_{f,MR} = [21\ 22\ 25\ 26]$ are chosen to be included in the mathematical model. These are some flexible modes belonging to the foundation, which are found to influence the dynamical behaviour of the combined rotor-bearing-foundation dynamics for the high-speed blower system. To describe the coil dynamics, the state space representation in equation (16) is used. The representation is established with the matrices from equation (15) and is valid for one coil in the electromagnet.

$$A_{c,ss} = -\frac{R}{L}, \qquad \mathbf{B}_{c,ss} = \begin{bmatrix} \frac{1}{L} & -\frac{k_u}{L} \end{bmatrix}, \qquad C_{c,ss} = 1, \qquad \mathbf{D}_{c,ss} = [0 \quad 0] \quad (15)$$

$$\mathbf{G}_{c,ss} = \begin{cases} \dot{x}_{c,ss} = A_{c,ss}x_{c,ss} + \mathbf{B}_{c,ss}\mathbf{u}_{c,ss} \\ \mathbf{y}_{c,ss} = C_{c,ss}x_{c,ss} + \mathbf{D}_{c,ss}\mathbf{u}_{c,ss} \end{cases} \quad (16)$$

The coefficients, L ,k_u, k_i, and k_s are linearized for the expected position of the shaft during operation. A value for k_{Axial} has been obtained from a study using COMSOL for the passive magnet rings moving in a radial direction. In the study, it is assumed that the reaction is linearly dependent on the relative displacement between the magnet rings. In equation (17), the estimations for the coefficients are presented.

$$L = \frac{\mu_0 N^2 A}{2x_0}, \qquad k_u = \frac{\mu_0 N^2 A i_0}{2x_0^2}, \qquad k_i = \frac{\mu_0 N^2 A i_0}{x_0^2}, \qquad k_s = \frac{\mu_0 N^2 A i_0^2}{x_0^3}, \qquad k_{Axial} = 19\left[\frac{\mathrm{kN}}{\mathrm{m}}\right] \quad (17)$$

For the sensors, a first or second order Butterworth filter is used depending on the implemented control scheme. The control object is obtained from combining the components as presented in figure 2. The resulting state space formulation is described in equation (18). The matrices $\mathbf{C}_{ss,obj}$ and $\mathbf{D}_{ss,obj}$ can be designed such that one obtains the desired output states from the control objective.

$$\mathbf{G}_{ss,obj} = \begin{cases} \dot{\mathbf{x}}_{ss,obj} = \mathbf{A}_{ss,obj}\mathbf{x}_{ss,obj} + \mathbf{B}_{ss,obj}\mathbf{u}_{ss,obj} \\ \mathbf{y}_{ss,obj} = \mathbf{C}_{ss,obj}\mathbf{x}_{ss,obj} + \mathbf{D}_{ss,obj}\mathbf{u}_{ss,obj} \end{cases} \quad (18)$$

The PID control scheme, presented in equation (19), is implemented utilizing a second order Butterworth filter for the position and current sensors in the global mathematical model.

$$G_{PID-scheme}(s) = K_p\left(1 + \frac{1}{\tau_i s} + \frac{\tau_d s}{\epsilon s + 1}\right)\left(\frac{s^2 + \omega_{0,1}^2}{s^2 + \frac{\omega_{0,1}}{Q}s + \omega_{0,1}^2}\right)\left(\frac{s^2 + \omega_{0,2}^2}{s^2 + \frac{\omega_{0,2}}{Q}s + \omega_{0,2}^2}\right) \quad (19)$$

Table 2: Values used in PID control scheme and current tracking controller.

Parameter	K_p	τ_i	τ_d	$\omega_{0,1}$	$\omega_{0,2}$	Q	K_{cur}	τ_{cur}
Value	$13\ \left[\frac{\mathrm{A}}{\mu\mathrm{m}}\right]$	0.3 [s]	2 [ms]	466 [Hz]	470 [Hz]	2 [−]	$500\ \left[\frac{\mathrm{Ticks}}{\mathrm{A}}\right]$	1 [s]

The output of the PID control scheme is the current reference which is tracked by a PI control design presented in equation (20).

$$G_{PI-scheme}(s) = K_{cur}\left(1 + \frac{1}{\tau_{cur}s}\right) \quad (20)$$

In table 2, the values used in the PID control scheme and current tracking control scheme are presented. The model-based control design implemented is based on the control object having first order Butterworth filters implemented on the sensor signals. For this control object, an observer in the form of a Kalman filter is used. Using an estimation of the process noise intensities, $\mathbf{V}_1$, and measurement noise intensities, $\mathbf{V}_2$, the Kalman filter gains can be computed from equation (21).

$$\mathbf{0} = \mathbf{A}_{ss,obj}\mathbf{Q} + \mathbf{Q}\mathbf{A}_{ss,obj}^{\mathrm{T}} + \mathbf{B}_{ss,obj}\mathbf{V}_1\mathbf{B}_{ss,obj}^{\mathrm{T}} - \mathbf{Q}\mathbf{C}_{ss,obj}^{\mathrm{T}}\mathbf{V}_2^{-1}\mathbf{C}_{ss,obj}\mathbf{Q}, \qquad \mathbf{L}_{Kal} = \mathbf{Q}\mathbf{C}_{ss,obj}^{\mathrm{T}}\mathbf{V}_2^{-1} \quad (\mathbf{21})$$

The model-based control scheme should include integral action on the position sensor signals. Therefore, the control object is augmented with integral states in equation (22). The controller gains are calculated in equation (23) based on weighting matrices for the states, $\mathbf{R}_1$, and the input, $\mathbf{R}_2$.

$$\mathbf{A}_{ss,obj,int} = \begin{bmatrix} \mathbf{A}_{ss,obj} & \mathbf{0} \\ -\mathbf{C}_{ss,obj} & \mathbf{0} \end{bmatrix}, \qquad \mathbf{B}_{ss,obj,int} = \begin{bmatrix} \mathbf{B}_{ss,obj} \\ \mathbf{0} \end{bmatrix} \quad (22)$$

$$\mathbf{0} = \mathbf{A}_{ss,obj,int}\mathbf{P} + \mathbf{P}\mathbf{A}_{ss,obj,int}^{\mathrm{T}} + \mathbf{R}_1 - \mathbf{P}\mathbf{B}_{ss,obj,int}\mathbf{R}_2\mathbf{B}_{ss,obj,int}^{\mathrm{T}}\mathbf{P}, \qquad \mathbf{K}_{Opt} = \mathbf{R}_2^{-1}\mathbf{B}_{ss,obj,int}^{\mathrm{T}}\mathbf{P} \quad (\mathbf{23})$$

Using the system augmented with integral states, the controller dynamics are built in line with the control architecture visualized in figure 2. Before implementation, the LQG control design is discretized, balanced, and reduced to fit the space requirements for the hardware installed in the test-facility. This reduction is based on keeping the most important singular values for the control design.

4 RESULTS

The mathematical model has been optimized using a least squares fit for the expected relative displacements between the rotor and foundation against the measured relative displacements as well as the expected current running in the coils against the measured current. The expected values are provided as outputs from the global mathematical model. The measured values are obtained with the PID control design implemented on the high-speed blower system. A comparison between the estimated frequency response from the control objective and the measured frequency response after the optimization is presented in figure 3. It is noticed that the control object does contain some regions where the estimation of the real plant is not completely in line with the experimentally obtained response, i.e. around 150 [Hz] and between 400 [Hz] to 500 [Hz]. However, the control plant does seem to include the most prominent responses and does seem to be able to sustain a model-based control design. In figure 4, the LQG control design is implemented to the experimental test facility. The experimentally obtained frequency response is compared to the estimated response from the control object applied with the LQG control design. The experimentally obtained frequency response for the system with the PID control scheme is plotted again for easier comparison. It is noted that the experimentally

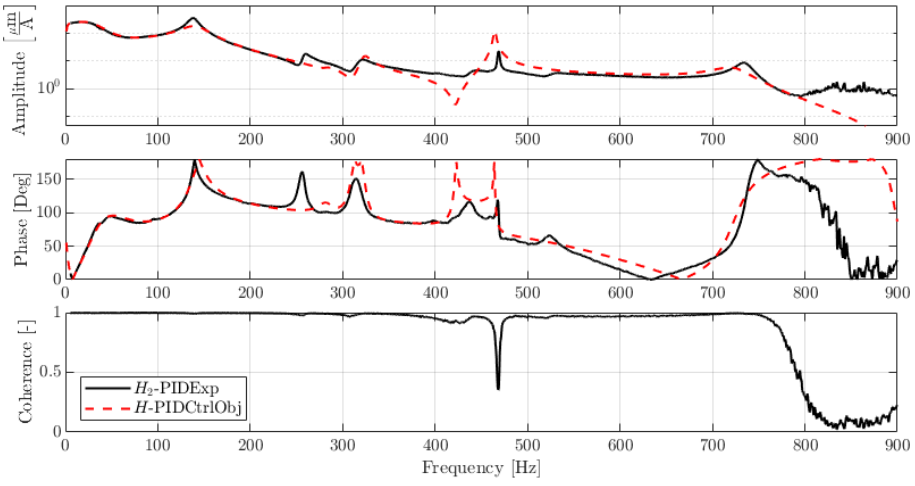

Figure 3: Experimentally obtained frequency response versus the estimated frequency response for the control object implemented with a PID control design.

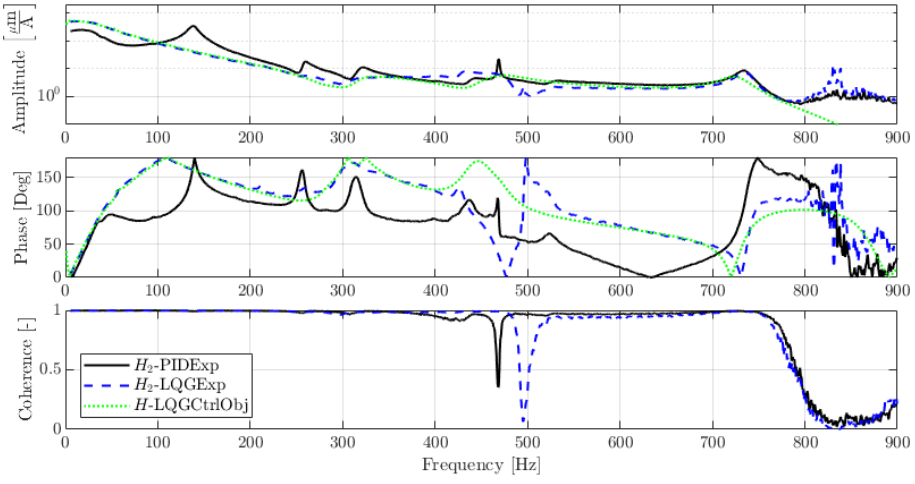

Figure 4: Experimentally obtained frequency response for PID control design versus the experimentally obtained frequency response for LQG control design and estimated frequency response for the control object.

obtained frequency response is well described by the expected frequency response in most of the frequency range. However, as it is for the control object applied with the PID control scheme as well, the amplification and phase shift are not well described in the frequency band from 400 [Hz] to 500 [Hz]. Comparing the experimental frequency response using the PID control scheme against the experimental frequency response using the LQG control design, it is noticed that while the response in the range from 0 [Hz] to 100 [Hz] has increased for the system with the LQG control design implemented, the response has either decreased or remained at the same level for the rest of the frequency band. Therefore, the method of including the foundation dynamics in the control design is deemed successful.

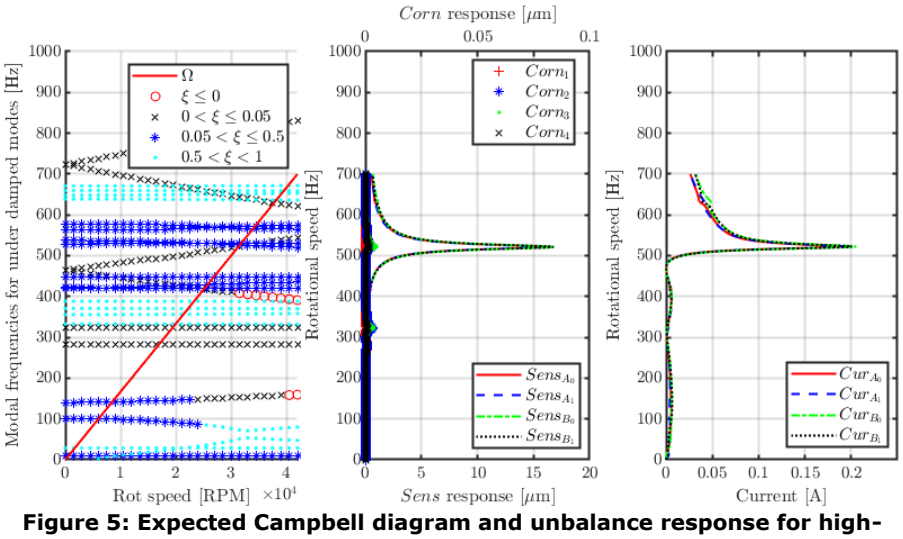

Figure 5: Expected Campbell diagram and unbalance response for high-speed blower using PID control scheme (Centre bottom: Rotor responses; Centre top: Foundation corner responses; Right bottom: Current in coils).

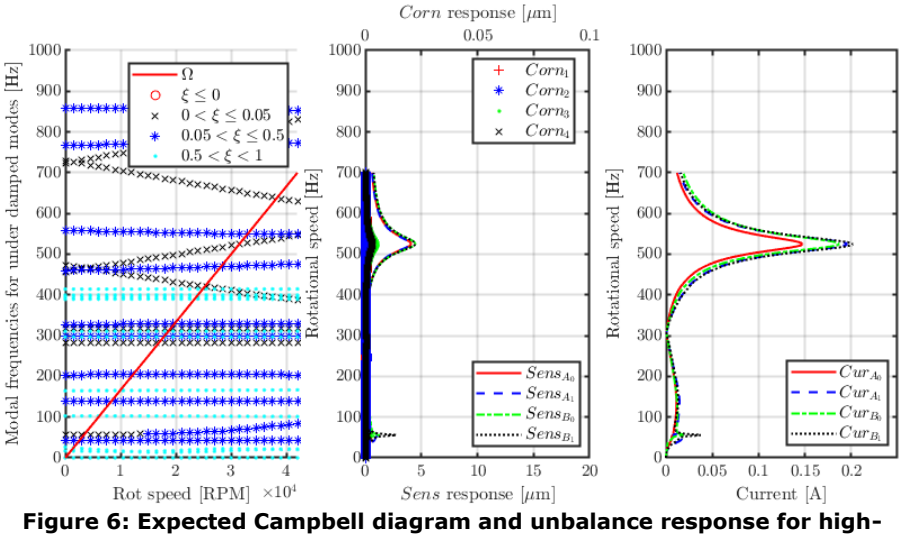

Figure 6: Expected Campbell diagram and unbalance response for high-speed blower using LQG control scheme (Centre bottom: Rotor responses; Centre top: Foundation corner responses; Right bottom: Current in coils).

In figures 5 and 6, two unbalance responses are calculated for the system having the two different control schemes implemented. The residual unbalance mass is assumed to be in the rotor laminates for the active magnetic bearing. Figure 5 shows a very high response peak at around 520 [Hz], which is coincident with the crossing of the forward whirl for the first flexible eigenmode for the shaft. It is noticed that no corners of the foundation are expected to generate a considerable response. However, it is also noticed that the mathematical model predicts the system to be unstable at around 31500 [RPM]. In figure 6, it is evident that the resonance peak caused by the crossing of the first flexible mode is reduced drastically but at the expense of some

additional undesired resonance peaks around 50 [Hz] and a slightly higher response in the corners of the t-slot plate. Analysing the expected amplification of the current in the coils, it is noticed that the limitations of the bearing design are complied with and that the amplification of the current around 520 [Hz] is distributed over a broader frequency range. Also, the control design is expected to be stable from the assessment of the damping factors of the eigenvalues. The increased response in the corners of the t-slot plate indicates that the LQG control algorithm is dissipating some of the energy from the first flexible mode for the shaft to the foundation, thereby exciting the foundation structure as well.

5 CONCLUSIONS

In this article, it has been illustrated that foundation dynamics can be included in a model-based control design such as an LQG control scheme. The method has been compared against a PID control scheme utilizing notch filters to stabilize the shaft.
It is found that some complications regarding undesired amplifications of the response occur when the foundation response is considered in the control design. However, the overall performance of the model-based control design appears to be superior to that of a decentralized PID control scheme.

REFERENCE LIST

(1) Schweitzer, G., Maslen, E. H., et al. (2009) "Magnetic Bearing: Theory, Design, and Application to Rotating Machinery". *Springer*, Berlin, Germany.

(2) Schweitzer, G. (2002) "Active magnetic bearings-chances and limitations". *6th International Conference on Rotor Dynamics*., 1-14.

(3) Filatov, A. & Hawkins, L. (2015) "Comparative study of axial/radial magnetic bearing arrangements for turbocompressor applications". *Proceedings of the Institution of Mechanical Engineers. Part I: Journal of Systems and Control Engineering*, **230**(4), 300-310.

(4) Tondl, A. (1960) "The stability of motion of a rotor with unsymmetrical shaft on an elastically supported mass foundation". *Ingenieur-Archiv*, **29**(6), 410-418.

(5) Gasch, R. (1976) "Vibration of large turbo-rotors in fluid-film bearings on an elastic foundation". *Journal of Sound and Vibration*, **47**(1), 53-73.

(6) Mourelatos, Z. P. & Parsons, M. G. (1987) "A finite element analysis of beams on elastic foundation including shear and axial effects". *Computers and Structures*, **27**(3), 323-331.

(7) Ruijgrok, M., Tondl, A. & Verhulst, F. (1993) "Resonance in a rigid rotor". *Zamm*, **73**(10), 255-263.

(8) Dagnaes-Hansen, N. A. & Santos, I. F. (2019) "Magnetically suspended flywheel in gimbal mount - test bench design and experimental validation". *Journal of Sound and Vibration*, **448**, 197-210.

(9) Paulsen, T. T. (2018) "Modelling, Design, Implementation and Experimental Testing of Flexible Rotors on Active Magnetic Bearings Considering Flexible Foundations". MS Thesis, Technical University of Denmark, Kgs. Lyngby, Denmark, June.

(10) Lauridsen, J. S. & Santos, I. F. (2018) "On-site identification of dynamic annular seal forces in turbo machinery using active magnetic bearings: An experimental investigation". *Journal of Engineering for Gas Turbines and Power*, **140**(8), 1-9.

(11) Nelson, H. D. (1980) "A finite rotating shaft element using Timoshenko beam theory". *Journal of Mechanical Design*, **102**(4), 793-803.